Increased stiffness and flow resistance of the inner wall of Schlemm's canal in glaucomatous human eyes

Amir Vahabikashi[a], Ariel Gelman[b], Biqin Dong[a,c], Lihua Gong[b], Elliott D. K. Cha[b], Margit Schimmel[d], Ernst R. Tamm[d], Kristin Perkumas[e], W. Daniel Stamer[e,f], Cheng Sun[c], Hao F. Zhang[a,g], Haiyan Gong[b], and Mark Johnson[a,c,g,1]

[a]Department of Biomedical Engineering, Northwestern University, Evanston, IL 60201; [b]Department of Ophthalmology, Boston University School of Medicine, Boston, MA 02118; [c]Department of Mechanical Engineering, Northwestern University, Evanston, IL 60201; [d]Institute of Anatomy, University of Regensburg, D-93053 Regensburg, Germany; [e]Department of Ophthalmology, Duke University, Durham, NC 27710; [f]Department of Biomedical Engineering, Duke University, Durham, NC 27708; and [g]Department of Ophthalmology, Northwestern University, Chicago, IL 60611

Edited by Ian A. Sigal, University of Pittsburgh, Pittsburgh, PA, and accepted by Editorial Board Member Jeremy Nathans November 7, 2019 (received for review July 11, 2019)

The cause of the elevated outflow resistance and consequent ocular hypertension characteristic of glaucoma is unknown. To investigate possible causes for this flow resistance, we used atomic force microscopy (AFM) with 10-μm spherical tips to probe the stiffness of the inner wall of Schlemm's canal as a function of distance from the tissue surface in normal and glaucomatous postmortem human eyes, and 1-μm spherical AFM tips to probe the region immediately below the tissue surface. To localize flow resistance, perfusion and imaging methods were used to characterize the pressure drop in the immediate vicinity of the inner wall using giant vacuoles that form in Schlemm's canal cells as micropressure sensors. Tissue stiffness increased with increasing AFM indentation depth. Tissues from glaucomatous eyes were stiffer compared with normal eyes, with greatly increased stiffness residing within ∼1 μm of the inner-wall surface. Giant vacuole size and density were similar in normal and glaucomatous eyes despite lower flow rate through the latter due to their higher flow resistance. This implied that the elevated flow resistance found in the glaucomatous eyes was localized to the same region as the increased tissue stiffness. Our findings implicate pathological changes to biophysical characteristics of Schlemm's canal endothelia and/or their immediate underlying extracellular matrix as cause for ocular hypertension in glaucoma.

primary open-angle glaucoma | extracellular matrix | biophysics

Aqueous humor, which is secreted into the eye by the ciliary epithelia posterior to the iris, provides nutrition and oxygen to the avascular anterior segment tissues of the eye. Known as the conventional outflow pathway, the primary route of drainage for aqueous humor from the eye is 1) through the trabecular meshwork, the deeper aspects of which are known as the juxtacanalicular connective tissue, 2) through giant vacuoles and micrometer-sized openings called "pores" in the inner-wall endothelium lining of Schlemm's canal, 3) circumferentially through Schlemm's canal lumen, and 4) finally into the collector channels and aqueous veins that drain the aqueous humor back into the venous system (Fig. 1). Primary open-angle glaucoma, a leading cause of blindness, is often associated with an elevated intraocular pressure caused by increased resistance to the flow of aqueous humor through the conventional outflow pathway (1, 2). Determining the cause of this pathological increase in flow resistance has vexed scientists.

Studies suggest that changes to the endothelial lining of Schlemm's canal and/or adjacent extracellular matrix in the juxtacanalicular connective tissue are responsible for the elevated flow resistance characteristic of glaucoma (3–6). The density of micrometer-sized pores in the inner-wall endothelium of Schlemm's canal is reduced in glaucoma (7, 8), and Schlemm's canal endothelial cells cultured from glaucomatous eyes form fewer pores than cells from normal eyes (9). Other studies show that the stiffness of the trabecular meshwork and cultured Schlemm's canal endothelial cells are both altered in glaucoma (9–12).

We here report the results of studies designed to localize and quantify stiffness and outflow resistance changes in glaucomatous eyes using atomic force microscopy (AFM), perfusion, and morphological examination. We used AFM to characterize the stiffness of both Schlemm's canal endothelial cells and their substrate in normal and glaucomatous human eyes. To this end, we varied tip size and indentation depth to determine depth-dependent stiffness in the tissue. Since giant vacuoles in Schlemm's canal endothelial cells form in a pressure-dependent fashion (13), we used the density and size of these giant vacuoles as microsensors of transcellular pressure drop, comparing normal and glaucomatous human eyes perfused at the same intraocular pressure.

Using AFM, we found dramatically increased stiffness in the glaucomatous inner-wall tissue that is localized very near the surface of the tissue where the Schlemm's canal endothelial cells and their immediate underlying extracellular matrix reside. Surprisingly, we found the density and size of giant vacuoles to be similar comparing normal with glaucomatous eyes. Combining these observations, we concluded that the increased flow resistance of glaucomatous eyes occurs in the immediate vicinity of the inner-wall endothelium of Schlemm's canal. This increased flow resistance may be the result of the increased stiffness of the endothelial cells themselves, their immediate underlying extracellular matrix (e.g., basal lamina), or both.

Significance

Glaucoma is a leading cause of irreversible blindness. The elevated intraocular pressure that is characteristic of primary open-angle glaucoma is due to increased resistance to aqueous humor outflow. Localizing this increased resistance has eluded investigators until recently. We report here that the glaucomatous flow resistance can be found within approximately 1 μm of the surface of the endothelial lining of Schlemm's canal in the aqueous humor outflow pathway of the eye. There is a greatly increased tissue stiffness in this same narrow region. Exploring and targeting these highly localized biophysical changes will allow development of new therapies for glaucoma.

Author contributions: A.V., A.G., W.D.S., H.F.Z., H.G., and M.J. designed research; A.V., A.G., B.D., L.G., E.D.K.C., M.S., E.R.T., K.P., and H.G. performed research; E.R.T., W.D.S., C.S., H.F.Z., H.G., and M.J. contributed new reagents/analytic tools; A.V., A.G., K.P., H.G., and M.J. analyzed data; and A.V., A.G., B.D., E.R.T., W.D.S., C.S., H.F.Z., H.G., and M.J. wrote the paper.

The authors declare no competing interest.

This article is a PNAS Direct Submission. I.A.S. is a guest editor invited by the Editorial Board.

[1]To whom correspondence may be addressed. Email: m-johnson2@northwestern.edu.

This article contains supporting information online at https://www.pnas.org/lookup/suppl/doi:10.1073/pnas.1911837116/-/DCSupplemental.

First published December 5, 2019.

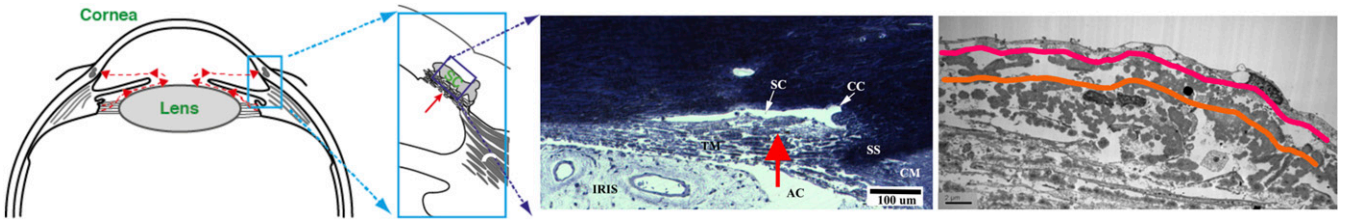

Fig. 1. Aqueous humor outflow pathway is shown schematically (*Left*) (9). Light micrograph of this tissue (*Middle*). Transmission electron micrograph of the inner-wall region of Schlemm's canal (SC) (*Right*). Aqueous humor flows (red arrows) from the anterior chamber (AC) to the trabecular meshwork (TM), into Schlemm's canal and then enters collector channels (CC) spaced periodically around the eye. From here, the aqueous humor flows into the episcleral veins. CM, ciliary muscle; SS, scleral spur. The 2 colored lines (*Right*) are 1 μm (magenta) and 3 μm (orange) from Schlemm's canal and represent approximate boundaries of the regions probed by the 1- and 10-μm AFM probes, respectively (*Discussion*). (Scale bars, 100 μm [*Middle*] and 2 μm [*Right*].)

Results

Schlemm's Canal Cells and Their Substrate Have Increased Stiffness in Glaucoma. Fifteen normal and 8 glaucomatous postmortem human eyes were obtained from eye banks (*SI Appendix*, Table S1). Aqueous humor outflow resistance was significantly increased in the glaucomatous as compared with normal eyes (9.1 ± 1.4 vs. 4.1 ± 0.45 mm Hg·μL^{-1}·min, respectively; $P < 0.02$) (Table 1). There were fewer optic nerve axons in glaucomatous eyes compared with normal eyes (232,126 ± 70,401 vs. 435,024 ± 79,408) although there was high variability and difference did not quite reach statistical significance ($P < 0.08$) (Table 1). Optic nerve count decreased with increasing outflow resistance ($P < 0.04$, $r = -0.62$).

AFM with a 10-μm spherical tip was used to measure the elastic modulus of specimens of the inner wall of Schlemm's canal (see details in *Materials and Methods*). The inner wall remained largely intact after dissection although occasional breaks were seen in the tissue (Fig. 2). Fig. 3 shows 5 typical patterns that were seen when AFM was used to measure the elastic modulus of the inner-wall tissue as a function of indentation. Most plots showed either 1 (Fig. 3 *A*, *C*, and *D*) or 2 plateaus (Fig. 3*B*) where modulus was relatively independent of indentation. The average moduli of the plateaus that began in the first 100 nm of indentation were relatively low (<1 kPa) (e.g., Fig. 3*A*; first plateau of Fig. 3*B*) and were designated as E_1; the average moduli of plateaus that began at deeper indentations and had higher values

Table 1. Measurements of tissue stiffness using 1- and 10-μm AFM tips in normal and glaucomatous eyes

			Tip size (10 μm)			Tip size (1 μm)		
ID	Outflow resistance	Axon count	E_1	E_2	E_{last}	E_1	E_2	E_{last}
Normal eyes								
1	NA	212,999	0.65	7.01	11.34			
2	NA	266,095	0.39	2.65	1.48			
3	NA	401,778	0.39	5.55	5.87			
4	NA	461,013	0.6	9.08	9.82			
5	NA	NA	0.48	5.17	3.09			
6	4.17	287,739	0.28	6.43	1.89			
7	NA	1,084,664	0.24	0.94	0.87			
8	2.50	NA*	0.09	7.88	1.27			
9	2.94	765,436	0.14	6.92	10.29			
10	NA	359,003	0.33	12.9	22.26			
11	5.26	288,568	0.51	2.57	6.85			
12	5.88	253,525	0.2	16.59	8.86			
13	3.85	404,445	0.91	9.19	10.25			
14	NA	NA	0.71	14.5	12.9	0.49	6.73	9.95
15	4.00	NA	0.7	4.86	7.28	0.46	7.9	13.7
Mean	4.09	435,024	0.44	7.48	7.62	0.48	7.32	11.83
SE	0.42	75,712	0.06	1.11	1.43	0.01	0.41	1.33
Glaucomatous eyes								
16	11.11	7,327	0.92	10.77	11.48			
17	6.25	206,466	0.70	3.06	5.27			
18	8.33	136,713	0.77	9.88	13.26			
19	9.09	363,394	0.84	4.64	4.71			
20	NA	NA	0.56	11.26	11.41			
21	5.88	575,444	0.66	10.07	17.86			
22	16.67	120,415	0.97	5.02	5.2	0.43	23.6	28.77
23	6.67	215,122	0.52	20.12	24.15	0.62	108.67	79.04
Mean	9.14	232,126	0.74	9.35	11.67	0.53	66.14	53.91
SE	1.33	77,120	0.05	1.78	2.26	0.07	30.08	17.77

NA, not available.
*Low axons due to cancer.

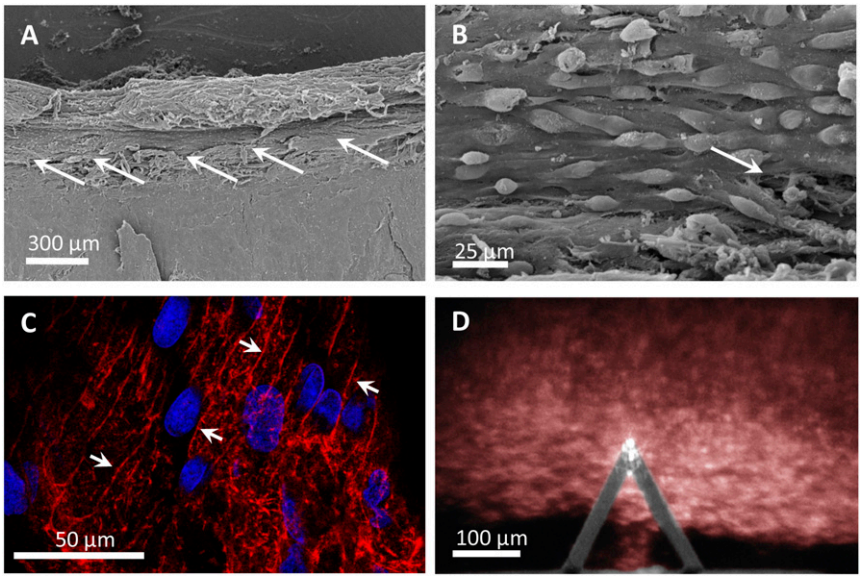

Fig. 2. Images of extracted tissue. (*A*) Scanning electron micrograph of extracted tissue showing the inner wall of Schlemm's canal (arrows). (*B*) Higher magnification showing the inner-wall tissue. Bulges are nuclei of the Schlemm's canal endothelial cells, and the arrow shows a tear in tissue likely made during tissue extraction. (*C*) Confocal image of the inner-wall endothelium demonstrates a similar cell pattern as the electron micrograph; nuclei (blue) and F-actin (red) show stretched cell layout and their peripheral cortices (arrows). (*D*) AFM probe indenting the tissue that is illuminated from below.

(>2 kPa) (e.g., second plateau of Fig. 3 *B* and *D*) were designated as E_2; details are given in *Materials and Methods*. Some plots (Fig. 3*E*) showed no plateaus, and for such plots, no values for E_1 or E_2 were calculated. For all plots, the modulus measured at deepest indentation was designated as E_{last}. E_1 was interpreted as the modulus of the Schlemm's canal cells that lies on the surface of the tissue samples, while E_2 was associated with the substrate of these cells.

E_1 (0.74 ± 0.06 kPa) in glaucomatous eyes was significantly higher ($P < 0.003$) than in normal eyes (0.44 ± 0.06 kPa) (Fig. 4*A*). E_2 (9.35 ± 1.90 kPa) and E_{last} (11.67 ± 2.42 kPa) were also higher in glaucomatous eyes than normal eyes (7.48 ± 1.14 and 7.62 ± 1.48 kPa, respectively) but these differences were not statistically significant ($P > 0.15$). We did not find a significant correlation between E_1 and E_2 or E_1 and E_{last} ($P > 0.3$).

Outflow resistance increased significantly with E_1 (Fig. 4*B*; $P = 0.01$, $r = 0.66$) but was not correlated with E_2 or E_{last} ($P > 0.8$). Optic nerve counts decreased with an increase in E_1 ($P < 0.03$, $r = -0.58$) (Fig. 4*C*); no correlation was found between either E_2 or E_{last} and optic nerve count ($P > 0.2$).

There was no statistically significant effect of race (white vs. black) or gender on any of these results ($P > 0.15$). Outflow resistance increased with age ($P < 0.04$) as found in other studies (14), but no other measured variables correlated with age ($P > 0.3$). While postmortem time did not influence any of the statistically significant results ($P > 0.2$), postmortem time was positively correlated with E_2 ($P < 0.03$) and E_{last} ($P < 0.04$).

These AFM studies demonstrate that the stiffness of the inner wall of Schlemm's canal is increased in glaucoma. In particular, the increased stiffness manifests itself in measurements made closer to the surface of the tissue rather than its deeper aspects, a finding which we explore further below.

Increased Inner-Wall Stiffness Resides Immediately below the Surface of the Inner Wall of Schlemm's Canal. While our AFM results were roughly comparable with those of Wang et al. (12), showing that glaucomatous tissues are moderately stiffer than tissues from normal eyes, our results were markedly different from the AFM measurements by Last et al. (10), who reported that inner-wall tissue is an order of magnitude stiffer in glaucomatous eyes. A notable difference in the studies is that the AFM tip diameter used by our group and Wang et al. (10 μm) was much larger than that used by Last et al. (1 μm). As AFM tip diameter is reduced, the region of a tissue that is probed by the tip becomes progressively closer to the surface of that tissue (15–17). As such, we investigated the effect from AFM tip size (10 vs. 1 μm) in the last 2 normal and 2 glaucomatous eyes we examined.

In tissue from normal eyes, measurements of moduli vs. indentations were similar whether measured with 10- or 1-μm AFM tips (see Table 1 and a typical example in Fig. 4*D*). The behavior of glaucomatous tissue, however, was markedly different (e.g., Fig. 4*E*). For the first 100 nm of indentation, the modulus as measured with a 10-μm tip was similar to that measured with a 1-μm tip. However, with deeper indentations, the modulus of the glaucomatous tissue was much higher when measured with 1-μm tips than when measured with 10-μm tips.

Furthermore, consistent with the report of Last et al. (10), the values of E_2 and E_{last} measured with 1-μm AFM tips were much higher in the glaucomatous eyes than measured in the normal eyes. Last et al. found that E_{last} increased from an average value of 4.0 ± 2.2 kPa in normal eyes to 80.8 ± 32.5 kPa in glaucomatous eyes. Using 1-μm AFM tips, we found values of E_{last} increasing from 10.0 and 13.7 kPa in the 2 normal eyes we examined to 28.8 and 79.0 kPa in the 2 glaucomatous eyes. Our values in the 2 normal eyes are a little higher than those from Last et al., likely due to our greater depth of indentation, whereas the values in glaucomatous eyes are in the same range as reported by their group (29.6 to 138.4 kPa).

Taken together, we find much higher values of E_2 and E_{last} in glaucomatous eyes when measured with 1-μm than 10-μm AFM tips. This confirms our finding that the increased stiffness of the glaucomatous inner-wall tissue occurs in a region very near its surface. We were next interested to determine if this increased stiffness affects the pressure drop in this region.

The Increased Flow Resistance in Glaucomatous Eyes Is Generated at or Immediately below the Surface of the Inner Wall of Schlemm's Canal. Giant vacuoles are distensions of inner-wall endothelial cells into the lumen of Schlemm's canal (Fig. 5 *A* and *B*) that increase in size and number as intraocular pressure is increased

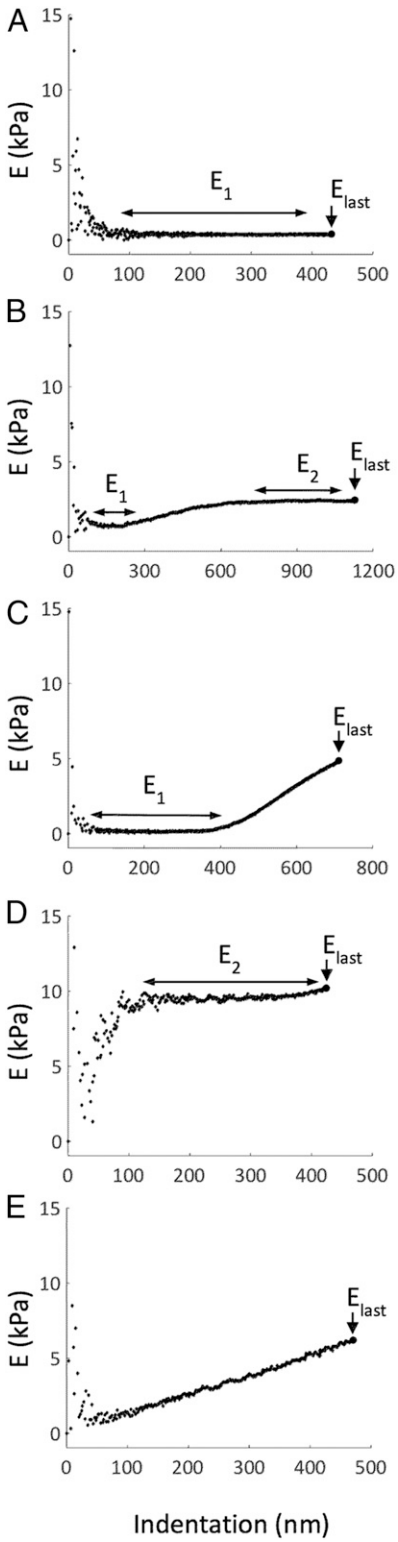

Fig. 3. Modulus (E) as a function of depth of AFM indentation into the tissue using a 10-μm AFM tip showing 5 different patterns (*A*–*E*). Each plot represents a single set of AFM measurements at 1 location. For a homogeneous material, the modulus would be independent of indentation depth. The common pattern of increasing values of E with indentation seen in *B*–*E* reflects the tissue being stiffer as the AFM tip probes deeper into the tissue. E_1 (interpreted as SC stiffness) and E_2 (interpreted as substrate stiffness) are average moduli of the plateaus seen in the results, determined as described in the text. E_{last} is the modulus measured at the deepest indentation.

(13, 18–20). Since giant vacuoles extend from the basal to the apical surface of the Schlemm's canal cells, their size is sensitive to the stiffness of these cells and the transcellular pressure drop across the cell. We aimed to use the size and density of these vacuoles as microsensors of transcellular pressure drop to characterize the local pressure drop across the inner wall of normal and glaucomatous eyes. To this end, we perfused enucleated human eyes at a constant pressure of 15 mm Hg followed by imaging studies to assess giant vacuole size and density in these eyes.

Six normal and 5 glaucomatous eyes were examined. Outflow resistance was significantly higher in the glaucomatous as compared with the normal group (38.4 ± 9.3 vs. 5.8 ± 0.9 mm Hg·μL^{-1}·min; $P < 0.03$). Fig. 5 *A* and *B* shows the typical morphology of the inner wall of Schlemm's canal of normal and glaucomatous eyes fixed at the same perfusion pressure (15 mm Hg). No obvious morphological difference in giant vacuoles was seen between normal and glaucomatous eyes. As noted previously (21), a higher fraction of Schlemm's canal was collapsed in glaucomatous as compared with normal eyes (19.6 vs. 6.3%, $P < 0.02$).

No obvious morphological difference in giant vacuoles could be detected between inactive and active flow regions in either normal or POAG eyes, nor were there statistically significant differences in any of the measured vacuole parameters between these 2 regions ($P > 0.4$; see details and interpretation in *SI Appendix*). Thus, data from inactive and active flow regions were pooled for all analyses reported here.

A total of 1,150 giant vacuoles were analyzed from 40 sections of normal eyes and 658 giant vacuoles were analyzed from 30 sections of glaucomatous eyes. The mean density of giant vacuoles along the length of the total Schlemm's canal was 13.9 ± 1.8 mm^{-1} for normal eyes and 14.1 ± 3.6 mm^{-1} for glaucomatous eyes. In open regions of Schlemm's canal, these densities were 14.9 ± 2.0 and 16.9 ± 3.5 mm^{-1}, respectively. These differences were not statistically significant ($P > 0.6$) (Fig. 5*C*).

The average size (cross-sectional area) of the giant vacuoles in glaucomatous eyes was 39.4 ± 9.8 μm^2, which was larger than the mean size of giant vacuoles in normal eyes (27.6 ± 4.8 μm^2); however, this difference was not statistically significance ($P > 0.3$) (Fig. 5*D*). The giant vacuole size distribution was positively skewed for normal (μ = 30.3 ± 1.4 μm^2, median 15.4 μm^2) and glaucomatous eyes (μ = 35.0 ± 1.8 μm^2, median 16.0) (Fig. 5*E*). Smaller giant vacuoles were more prevalent than larger ones in both normal and glaucomatous eyes. Other measurements of vacuoles can be found in *SI Appendix*.

There was no statistically significant effect of gender or postmortem time on any of these results ($P > 0.2$). Age was marginally related to outflow resistance ($P < 0.1$), as seen in the eyes used for our AFM studies, but no other measured variables ($P > 0.3$). Race could not be examined as all donors were Caucasian.

Together, the results from perfusion and imaging studies show that the size and density of giant vacuoles are similar in normal and glaucomatous eyes when perfused at the same intraocular pressure. This is surprising because the flow rates passing through the glaucomatous eyes were much lower than that passing through the normal eyes, due to a higher flow resistance of the former. In *Discussion*, we argue that these observations strongly imply that glaucomatous eyes have greatly increased flow resistance in the immediate vicinity of the inner wall of Schlemm's canal, where these vacuoles form.

Discussion

The elevated intraocular pressure characteristics of primary open-angle glaucoma have long been known to be caused by an increased resistance to the outflow of aqueous humor from the eye (1, 2). However, the locus of this flow resistance generation is still poorly understood (4, 5, 22). Here we report that both the

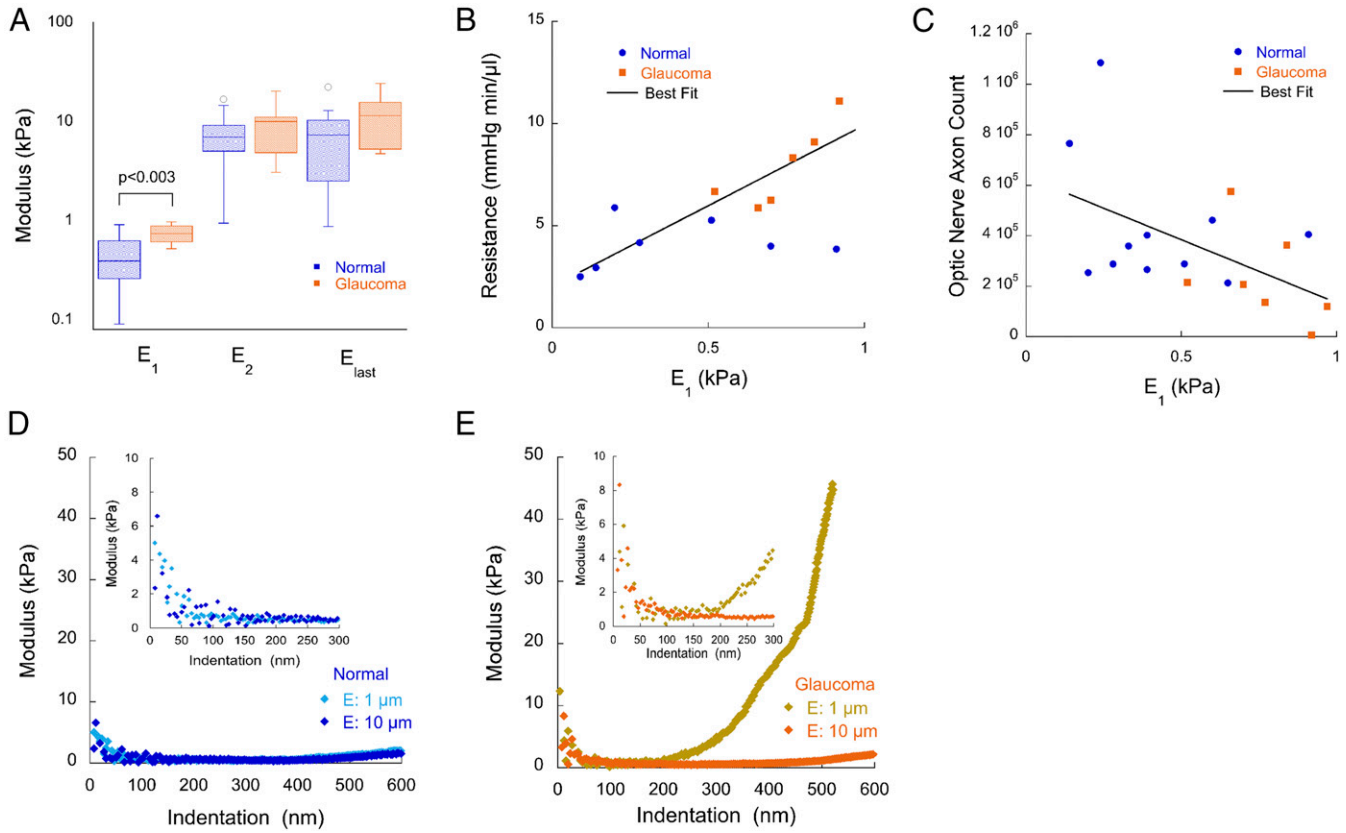

Fig. 4. Results from AFM measurements. (*A*) Box and whisker plots of elastic moduli of normal and glaucomatous inner-wall tissue as measured with a 10-µm AFM tip. (*B*) Outflow resistance (inverse outflow facility) of human eyes as a function of E_1 ($P < 0.02$) as measured with a 10-µm AFM tip. (*C*) Optic nerve counts of human eyes as a function of E_1 ($P < 0.03$) as measured with a 10-µm AFM tip. (*D* and *E*) Typical data for modulus as a function of indentation for inner-wall tissue from 1 normal and 1 glaucomatous eye as measured with a 1- or 10-µm AFM tip. (*D* and *E*, *Insets*) Regions where indentations are <300 nm.

stiffness and flow resistance of tissue in the immediate vicinity of the inner wall of Schlemm's canal are greatly increased in glaucomatous human eyes.

Using atomic force microscopy with a 10-µm spherical tip, we found that measurements of the elastic modulus (E_1) made near the surface of intact tissue from the inner wall of Schlemm's canal were higher ($P < 0.003$) in glaucomatous eyes ($E_1 = 0.7$ kPa) as compared with normal eyes (0.4 kPa). These moduli are in reasonable agreement with moduli measured in cultured glaucomatous and normal Schlemm's canal cells [1.2 and 0.8 kPa, respectively (9)]. We thus interpret our measurements of E_1 as characterizing the stiffness of the Schlemm's canal cells.

The finding of higher stiffness in glaucomatous Schlemm's canal cells in situ agrees with findings on Schlemm's canal cells in culture (9). We also found that the increased stiffness of the glaucomatous Schlemm's canal cells strongly correlated with the increased outflow resistance found in the glaucomatous eyes (Fig. 4*B*). Stamer et al. (23) proposed that the increased flow resistance in glaucoma results from decreased pore-forming capability of Schlemm's canal cells due to their elevated stiffness.

By pushing the AFM probe deeper, we were able to examine the stiffer tissue underneath the Schlemm's canal cells. Here, we found that the moduli (E_2 and E_{last}) of the glaucomatous tissue (9.4 and 11.7 kPa, respectively) were again higher than normal eyes (7.5 and 7.6 kPa), although these differences were not statistically significant. Wang et al. (12), using 10-µm AFM tips, also found an increase in glaucomatous inner-wall tissue (2.8 kPa) as compared with normal eyes (1.4 kPa), and the difference in their case was also not statistically significant. The lower values in their study, as compared with ours, are likely due to deeper indentation depth in our study used to measure E_2 and E_{last} (200 to 1,600 nm). We interpreted E_2 and E_{last} as characterizing the substrate under the Schlemm's canal cells.

Our results and those of Wang et al. using 10-µm AFM spherical tips differ markedly from AFM measurements reported by Last et al. (10) using a smaller spherical tip (1 µm). While their values in normal eyes (4.0 kPa) are between those measured by Wang et al. and those we report here, Last et al. found that glaucomatous inner-wall tissue was an order of magnitude stiffer (80.8 with a range of 29.6 to 138.4 kPa). We examined whether AFM tip size might explain the discrepancy. We found that the modulus of the inner-wall tissue in normal eyes was similar when measured with either a 1- or 10-µm diameter tip. However, in the case of glaucomatous inner-wall tissue, we found that the modulus was remarkably greater when measured with a 1-µm tip compared with when measured with 10-µm tips. We note that while our 1-µm results are based on only 2 normal and 2 glaucomatous eyes, they are in good agreement with results reported by Last et al. (10) and resolve a discrepancy in the literature (10, 12).

Tip size can profoundly affect the interpretation of AFM measurements. Vargas-Pinto et al. (16) found that sharp AFM tips characterize the cortex of a cell while larger, round tips characterize the deeper internal cytoskeleton. Vahabikashi et al. (15) and Lee et al. (17) investigated this more systematically and found that as the AFM tip size is reduced, the region of the cell/tissue probed becomes closer to the surface. The depth of the region probed scales with $\sqrt{\delta R}$, where δ is the indentation depth and R is the AFM tip radius (24) (Table 2). Thus, for a 200- to 400-nm indentation, we would anticipate that a 1-µm AFM tip

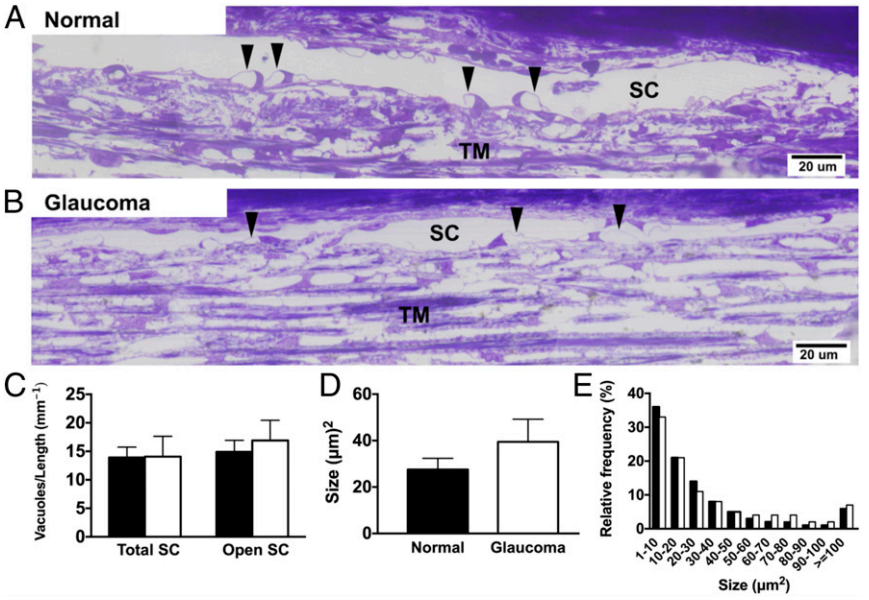

Fig. 5. Results from measurements of vacuolar parameters. (*A* and *B*) Representative images of the trabecular meshwork and inner wall of Schlemm's canal (SC) of a normal (77-y-old) and glaucomatous (63-y-old) eye. Images are composites of multiple images along the inner wall of SC. Vacuoles (arrowheads) are seen in both normal and diseased tissue. The canal in the normal eye is entirely open but partially collapsed in the glaucomatous eye. (*C*–*E*) Vacuole measurements in the SC comparing normal (filled) with glaucomatous (open) human eyes. (*C*) Density of giant vacuoles along the length of the SC (total SC) or along the open aspects (open SC). (*D*) Giant vacuole size. (*E*) Giant vacuole size distribution. None of the differences are statistically significant. Normal, filled; glaucomatous, empty; mean ± SE.

would probe tissue stiffness primarily in a region less than perhaps 1 μm from the tissue surface while a 10-μm tip would probe the region less than ~3 μm from the surface (Fig. 1, *Right*). Based on this, we interpret our findings to indicate that the greatly increased stiffness measured in the inner wall of glaucomatous eyes lies very near the surface of this tissue.

Our results differ from those of Camras et al. (11), who used uniaxial stretching to measure the tensile modulus of the trabecular meshwork and found it to be significantly decreased in glaucoma. Their results likely characterize the stiffness of the trabecular meshwork as a whole while our AFM measurements and those of Last et al. (10) are more reflective of the local tissue mechanics showing that the increased stiffness we measure is localized very near the inner wall of Schlemm's canal. Vranka et al. (25) used AFM and segmental flow studies to show that low-flow regions in the trabecular meshwork are associated with higher tissue stiffness than higher-flow regions. Wang et al. (12) also found higher stiffness in the low-flow regions using inverse finite-element modeling but found no significant differences using AFM. Raghunathan et al. (26) using AFM found much higher tissue stiffness in lower-flow regions of glaucomatous eyes than normal eyes. We did not examine segmental differences in tissue stiffness in high- vs. low-flow regions due to concerns that microspheres used to track segmental flow might otherwise affect the AFM measurements.

It is notable that the greatest increase in stiffness we found in the glaucomatous eyes, relative to normal eyes, was seen when the 1-μm AFM tip was pushed deeper than ~200 nm (Fig. 5*B* and 1-μm tip results in Table 1). This may be caused by extracellular matrix immediately underlying the Schlemm's canal cells [typical in vivo Schlemm's canal cell thickness is 0.2 to 1.5 μm (27, 28)]. One attractive candidate for this greatly stiffened layer is the basal lamina (and/or fibrillar extracellular matrix components attached to it) underlying the inner-wall endothelium of Schlemm's canal. Gong showed a decreased concentration of glycosaminoglycan in the basal lamina of the inner wall of Schlemm's canal of glaucomatous eyes (29). Overby et al. (30) showed that increased accumulation of basement membrane material underneath the Schlemm's canal cells in corticosteroid-induced glaucoma positively correlates with increased flow resistance. Increased stiffness of the basal lamina would both directly (31) and indirectly (32) increase the stiffness of the Schlemm's canal cells. Overby et al. (9) previously showed that Schlemm's canal cells are mechanosensitive to substrate stiffness and become stiffer when cultured on stiffer substrates in vitro.

The finding of increased tissue stiffness lying immediately adjacent to the inner wall of Schlemm's canal suggested that the increased resistance characteristic of glaucoma might also reside in this same region. To investigate this possibility, we used the giant vacuoles that form in Schlemm's canal cells as surrogate microsensors of transcellular pressure drop (13, 18–20). This was based on the findings of Grierson and Lee (13) that the size and density of giant vacuoles increase as intraocular pressure increases (up to 30 mm Hg; for higher pressures, vacuoles become constrained by the width of Schlemm's canal). We perfused normal and glaucomatous human eyes at a constant intraocular pressure (15 mm Hg) and compared the size and shape of giant vacuoles between them.

As expected, the flow resistances of the glaucomatous eyes were higher than those of normal eyes (Table 1), leading to significantly lower flow through these eyes, as all eyes were perfused at the same intraocular pressure. We were surprised to

Table 2. Estimate of the depth ($2\sqrt{\delta R}$) of the region probed by the AFM tip (from the surface of the inner wall of Schlemm's canal)

AFM tip diameter, nm (2*R*)	Indentation depth, nm (δ)	$2\sqrt{\delta R}$, nm
10	200	2,000
10	400	2,828
10	600	3,462
1	200	632
1	400	894
1	600	1,096

δ is the indentation depth, and *R* is the AFM tip radius.

find no significant differences in either vacuole size or density comparing normal with glaucomatous eyes (Fig. 5). A review of the literature revealed that a similar observation was reported in a meeting abstract 30 y ago.* We and others (10) found that inner-wall tissue is stiffer in glaucomatous eyes as compared with normal eyes. Since giant vacuole formation is a consequence of cell deformation caused by transcellular pressure drop, our measurements of similar vacuole size and density in normal and glaucomatous eyes imply that the transcellular pressure drop across the Schlemm's canal cells in glaucomatous eyes must be at least as high as or higher than that in normal eyes. As the glaucomatous eyes in our experiments had a much lower flow rate compared with the normal eyes, the transcellular flow resistance (ratio of transcellular pressure drop to the flow rate) must be greatly increased across the glaucomatous Schlemm's canal cells (and/or their basal lamina), consistent with a previous hypothesis (23).

An important limitation of our study involves the use of postmortem tissue. Unfortunately, postmortem tissue is rarely available within a few hours of death (33), and there is no animal model of primary open-angle glaucoma that recapitulates the known characteristics of the glaucomatous human trabecular meshwork (3). However, we note that we (and others) have used postmortem tissues to identify differences in mechanical properties between normal and glaucomatous tissues, and these differences need to be understood, even if there are some postmortem changes occurring in these tissues. It is also perhaps important here to point out that the trabecular meshwork is not a vascular tissue but instead gets the bulk of its energy by glycolysis rather than respiration (34). Thus, this tissue is less sensitive to loss of the vascular supply than other tissues. This, and the proximity of this tissue to atmospheric oxygen, is likely why this tissue has been successfully used for organ culture with intact inner-wall cells even though the tissue was collected many hours postmortem (35–38).

Our studies reveal significant biophysical changes to the outflow pathway in glaucoma, particularly a greatly increased stiffness of the endothelial cells lining the inner wall of Schlemm's canal and their immediate underlying tissue. This reconciles differences in measurements of the stiffness of the inner wall of Schlemm's canal, showing that AFM measurement techniques are sensitive to regional differences in tissue stiffness. Our studies also uncover a redistribution of aqueous outflow resistance in glaucoma with the increased flow resistance localized to the same region where increased tissue stiffness is measured.

Materials and Methods

Human Eyes. Postmortem human eyes without any known ocular diseases, other than cataract or primary open-angle glaucoma, were received from Eversight, the National Disease Research Interchange, or Miracles in Sight within 30 h postmortem. The characteristics of the eyes are listed in *SI Appendix*, Table S1.

Flow Resistance Measurements. Flow resistance through the aqueous outflow pathway (pressure drop/flow rate) was measured using established methods (39–43). For eyes used in the AFM studies, the eyes were perfused with Dulbecco's phosphate-buffered saline (DPBS) with 5.5 mM glucose (DBG) added at a constant pressure of 10 mm Hg using a syringe pump (Harvard Apparatus; Pump 11 Pico Plus Elite) controlled by a custom feedback control system (39, 40). The eye was placed in a beaker and covered with saline and moist tissue paper, and the beaker was placed in a water bath (34 °C). A perfusion needle (25-gauge) was placed into the posterior chamber of the enucleated eye and the perfusion was maintained until outflow resistance was constant for ∼30 min. Eyes used in the perfusion/imaging studies followed a similar protocol (41–43) but were perfused at 15 mm Hg.

Optic Nerve Axon Counts. To confirm glaucomatous damage to the optic nerve, optic nerve counts were done in some eyes used for the AFM studies. When available, optic nerve stumps were cut free from donor eyes, fixed in 2% paraformaldehyde/2.5% glutaraldehyde (pH 7.4), and sent in fixative to Germany. Upon arrival, the dura mater covering the stumps was removed and 1- to 2-mm-thick optic nerve slices were obtained by cross-sectioning. Slices were postfixed overnight in Karnovsky's fixative (44), incubated for 12 h in OsFe (1% OsO_4 and 0.8% potassium ferrocyanide in 0.1 M cacodylate buffer for 2 h at 4 °C) (45), and embedded in Epon. Semithin sections were cut on an ultramicrotome and stained with paraphenylenediamine as described previously (46). The total number of optic nerve axons was assessed using a modification of the protocol established by Quigley et al. (47). The total area of the cross-sectioned optic nerve was measured by tracing the outer edge of the nerve, excluding the meninges, at 200× magnification, followed by measuring the neuronal area and the area of connective tissue by tracing nerve fiber bundles and connective tissue septae, respectively. Measurements were done software-assisted on an Axio Imager Z1 (Zeiss) using the software ZEN and its module automatic measurement. In a subsequent step, each optic nerve cross-section was subdivided into 8 pie-shaped sectors. Axons were counted in five 32 × 32-μm sample areas (from central to peripheral) per sector at a magnification of 630× using an oil immersion lens. The estimation of the total nerve fiber count was then obtained by multiplying the mean value of the sample areas by the total area of the neuronal tissue. Thus, estimated axon counts are based on areal density measurements.

The axon count in 1 normal eye (no. 8) was not used in the statistical analysis as this eye had nonglaucomatous optic nerve damage that likely resulted from a tumor abutting the floor of the right middle cranial fossa.

AFM Measurements. The inner wall of Schlemm's canal was removed from enucleated human eyes following the procedure of Read et al. (48) (*SI Appendix*, Fig. S1). Tissue samples were examined in some cases using scanning electron microscopy and confocal microscopy (see *SI Appendix* for detailed methods). We note that, unlike the eyes used for vacuole size and density measurements (see below), these eyes were not perfused with microspheres to determine regions of active or inactive flow due to concern that the microspheres might otherwise affect the AFM measurements.

For AFM studies, inner-wall tissue samples, with the inner wall of Schlemm's canal facing upward, were mounted on positively charged SuperfrostPlus Gold slides (Thermo Fisher Scientific), allowing adhesive-free immobilization. Tissues were stained with a cell nucleus stain (NucRed Live 647; Thermo Fisher Scientific) and then rinsed with DPBS (Thermo Fisher Scientific).

Measurements of tissue stiffness were made on a BioScope Catalyst BioAFM (Bruker) with a home-built optical fluorescence microscope. Light from a mercury lamp (EL6000; Leica) passing through a 630-nm band-pass filter (ET630/20×; Chroma) was used to illuminate the tissue from the bottom. The fluorescence from the sample was passed through a 655-nm long-pass filter (ET655lp; Chroma) and imaged by an ultra-long working distance objective lens (10×, 0.28 NA, 34-mm WD; Mitutoyo) and a scientific CCD camera (Retiga; QImaging) placed above the atomic force microscope for multicontrast optical imaging.

Indentations for AFM measurements were performed using polystyrene spheres with a nominal diameter of either 1 or 10 μm mounted on a silicon nitride cantilever with a nominal spring constant of 0.06 N/m (PT.PS; Novascan Technologies). The deflection sensitivity and spring constant k were calibrated before each experiment using the thermal tune method (15). A ramp speed of 1 μm/s was used. We have previously shown (16) that this speed is sufficiently slow such that our measurements are not rate-dependent. For all samples, the tip traveled along the length and width of the tissue to probe multiple distinct sites. Single indentations were done on at least 20 locations using indentation depths that varied between 200 and 1,600 nm.

For all measurements, raw AFM data were used to calculate the force vs. indentation curve (see details in *SI Appendix*). The elastic modulus (E), as a function of indentation (δ), was then determined at each point of the force vs. indentation curve as follows (49):

$$E = \frac{3F(1-\nu^2)}{4R^{1/2}\delta^{3/2}}, \quad [1]$$

where R is the tip radius, and $\nu = 0.5$ is the Poisson ratio (50–52).

*A. de Kater, R. Allingham, D. L. Epstein, "Light microscopic quantitation of endothelial vacuoles and nuclei in Schlemm's canal in normal and glaucomatous human eyes," Association for Research in Vision and Ophthalmology (ARVO) (Investigative Ophthalmology & Visual Science, Sarasota, FL, 1989).

Calculated values of E_1, E_2, and E_{last} for each plot correspond to a single AFM indentation. E_1 and E_2 were average values for plateaus in which the modulus did not vary with indentation by more than roughly 5%. The modulus measured at the deepest indentation was designated E_{last}.

Vacuole Size and Density Measurements. Five glaucomatous eyes from 3 donors (63 to 81 y old) with clinically confirmed diagnoses of primary open-angle glaucoma and 6 age-matched normal eyes from 3 donors (64 to 78 y old) were examined. Eyes were perfused with DBG at 15 mm Hg to establish baseline outflow resistance. The anterior chambers were then exchanged (5 mL) and perfused with a fixed volume (200 μL) of DBG containing carboxylated polystyrene fluorescent microspheres (0.002% vol/vol, 500 nm; Life Technologies) at 15 mm Hg to label the flow pattern in the aqueous outflow pathway, and finally perfusion fixed at 15 mm Hg with modified Karnovsky's fixative (2.5% glutaraldehyde and 2% paraformaldehyde in a 0.1 M sodium phosphate buffer, pH 7.3) for 30 min. Upon completion of perfusion, a cut was made along the equator, and the eyes were immersed in the same fixative overnight.

The anterior segment of each eye was obtained and globally imaged using a previously established protocol (43). Each segment was then dissected radially into 16 wedges, from which the frontal sections were cut and imaged with a confocal microscope (Axiovert LSM 700; Carl Zeiss). Sections were assigned to either active or inactive flow regions based on the amount of fluorescent tracer visible along the trabecular meshwork and inner wall of Schlemm's canal (see details in *SI Appendix*).

After confocal imaging, frontal sections were postfixed with 2% osmium tetroxide in 1.5% potassium ferrocyanide for 2 h, dehydrated in an ascending series of ethanols, and embedded in Epon-Araldite (Electron Microscopy Sciences). Semithin sections (2 μm) of trabecular meshwork were cut, stained with 1% toluidine blue, and imaged by a light microscope (400×) (Olympus; FSX100).

The length of Schlemm's canal in each micrograph and the size and density of the giant vacuoles were determined from light microscopy images using ImageJ (NIH) (*SI Appendix*, Fig. S2*C*). The area (μm^2), perimeter (μm), major and minor axes (μm), and Feret's diameter (μm) were measured for each vacuole. Details are provided in *SI Appendix*.

Statistical Methods. All statistical analyses were done using JMP Pro-13 except for correlation coefficients that were done using Excel. The measurements of tissue stiffness were not normally distributed but instead showed a log-normal distribution such as is also seen in studies of cell stiffness (16, 53–55). As such, all AFM data were logarithmically transformed for statistical analysis and determined as geometric means ± SE around the geometric mean for each individual examined (9); averages taken over individuals were arithmetic. All measurements of giant vacuole parameters (e.g., density, size, perimeter, major/minor axes, and Feret's diameter), outflow facility, and optic nerve axon counts were arithmetic means for each eye and are reported as mean ± SE. Two-sided Student *t* tests with unequal variance were used for comparison between normal and glaucomatous populations, using Tukey to account for multiple comparisons.

Regression analysis was used to ascertain the effects of continuous variables or multiple variables. For multivariate regression, a forward regression analysis was used to determine which variables to include. A significance level of 0.05 was used; the minimum reported *P* value is 10^{-4}.

All data are available in the manuscript or in *SI Appendix*.

ACKNOWLEDGMENTS. We thank Dr. Thomas Read, then in the laboratory of Dr. John Flanagan at Toronto Western Hospital and now at Georgia Tech, who taught one of us (A.V.) the extraction procedure for removal of the inner wall of Schlemm's canal. We also gratefully acknowledge helpful conversations with Prof. Ross Ethier at Georgia Tech, and support from NIH EY019696 and EY022634 and The Massachusetts Lions Eye Research Fund.

1. T. Leber, Studien über den Flüssigkeitswechsel im Auge. *Albrecht Von Graefes Arch. Ophthalmol.* **19**, 87–106 (1873).
2. W. M. Grant, Clinical measurements of aqueous outflow. *AMA Arch. Opthalmol.* **46**, 113–131 (1951).
3. M. Johnson, K. Erickson, "Mechanisms and routes of aqueous humor drainage" in *Principles and Practice of Ophthalmology*, D. M. Albert, F. A. Jakobiec, Eds. (WB Saunders, Philadelphia, 2000), **vol. 4** Glaucoma, chap. 193B, pp. 2577–2595.
4. M. Johnson, What controls aqueous humour outflow resistance? *Exp. Eye Res.* **82**, 545–557 (2006).
5. W. D. Stamer, T. S. Acott, Current understanding of conventional outflow dysfunction in glaucoma. *Curr. Opin. Ophthalmol.* **23**, 135–143 (2012).
6. J. A. Vranka, M. J. Kelley, T. S. Acott, K. E. Keller, Extracellular matrix in the trabecular meshwork: Intraocular pressure regulation and dysregulation in glaucoma. *Exp. Eye Res.* **133**, 112–125 (2015).
7. R. R. Allingham *et al*., The relationship between pore density and outflow facility in human eyes. *Invest. Ophthalmol. Vis. Sci.* **33**, 1661–1669 (1992).
8. M. Johnson *et al*., The pore density in the inner wall endothelium of Schlemm's canal of glaucomatous eyes. *Invest. Ophthalmol. Vis. Sci.* **43**, 2950–2955 (2002).
9. D. R. Overby *et al*., Altered mechanobiology of Schlemm's canal endothelial cells in glaucoma. *Proc. Natl. Acad. Sci. U.S.A.* **111**, 13876–13881 (2014).
10. J. A. Last *et al*., Elastic modulus determination of normal and glaucomatous human trabecular meshwork. *Invest. Ophthalmol. Vis. Sci.* **52**, 2147–2152 (2011).
11. L. J. Camras, W. D. Stamer, D. Epstein, P. Gonzalez, F. Yuan, Circumferential tensile stiffness of glaucomatous trabecular meshwork. *Invest. Ophthalmol. Vis. Sci.* **55**, 814–823 (2014).
12. K. Wang *et al*., Estimating human trabecular meshwork stiffness by numerical modeling and advanced OCT imaging. *Invest. Ophthalmol. Vis. Sci.* **58**, 4809–4817 (2017).
13. I. Grierson, W. R. Lee, Light microscopic quantitation of the endothelial vacuoles in Schlemm's canal. *Am. J. Ophthalmol.* **84**, 234–246 (1977).
14. D. Gaasterland *et al*., Studies of aqueous humour dynamics in man. VI. Effect of age upon parameters of intraocular pressure in normal human eyes. *Exp. Eye Res.* **26**, 651–656 (1978).
15. A. Vahabikashi *et al*., Probe sensitivity to cortical versus intracellular cytoskeletal network stiffness. *Biophys. J.* **116**, 518–529 (2019).
16. R. Vargas-Pinto, H. Gong, A. Vahabikashi, M. Johnson, The effect of the endothelial cell cortex on atomic force microscopy measurements. *Biophys. J.* **105**, 300–309 (2013).
17. J. J. Lee, S. Rao, G. Kaushik, E. U. Azeloglu, K. D. Costa, Dehomogenized elastic properties of heterogeneous layered materials in AFM indentation experiments. *Biophys. J.* **114**, 2717–2731 (2018).
18. W. R. Lee, I. Grierson, Pressure effects on the endothelium of the trabecular wall of Schlemm's canal: A study by scanning electron microscopy. *Albrecht Von Graefes Arch. Klin. Exp. Ophthalmol.* **196**, 255–265 (1975).
19. I. Grierson, W. R. Lee, Pressure effects on flow channels in the lining endothelium of Schlemm's canal. A quantitative study by transmission electron microscopy. *Acta Ophthalmol. (Copenh.)* **56**, 935–952 (1978).
20. W. R. Lee, I. Gierson, Pressure effects on the flow channels in the lining endothelium of Schlemm's canal. A quantiative study by TEM. *Acta Ophthamologica* **91**, 88–105 (1978).
21. R. R. Allingham, A. W. de Kater, C. R. Ethier, Schlemm's canal and primary open angle glaucoma: Correlation between Schlemm's canal dimensions and outflow facility. *Exp. Eye Res.* **62**, 101–109 (1996).
22. D. W. Abu-Hassan, T. S. Acott, M. J. Kelley, The trabecular meshwork: A basic review of form and function. *J. Ocul. Biol.*, 10.13188/2334-2838.1000017 (29 July 2014).
23. W. D. Stamer *et al*., Biomechanics of Schlemm's canal endothelium and intraocular pressure reduction. *Prog. Retin. Eye Res.* **44**, 86–98 (2015).
24. E. Moeendarbary *et al*., The cytoplasm of living cells behaves as a poroelastic material. *Nat. Mater.* **12**, 253–261 (2013).
25. J. A. Vranka *et al*., Biomechanical rigidity and quantitative proteomics analysis of segmental regions of the trabecular meshwork at physiologic and elevated pressures. *Invest. Ophthalmol. Vis. Sci.* **59**, 246–259 (2018).
26. V. K. Raghunathan *et al*., Glaucomatous cell derived matrices differentially modulate non-glaucomatous trabecular meshwork cellular behavior. *Acta Biomater.* **71**, 444–459 (2018).
27. R. Vargas-Pinto, J. Lai, H. Gong, C. R. Ethier, M. Johnson, Finite element analysis of the pressure-induced deformation of Schlemm's canal endothelial cells. *Biomech. Model. Mechanobiol.* **14**, 851–863 (2015).
28. J. Lai *et al*., The role of Schlemm's canal endothelium cellular connectivity in giant vacuole formation: A 3D electron microscopy study. *Invest. Ophthalmol. Vis. Sci.* **60**, 1630–1643 (2019).
29. H. Gong, "Age-related changes in extracellular matrix components of the human aqueous outflow pathway," PhD thesis, Boston University, Boston, MA (1991).
30. D. R. Overby *et al*., Ultrastructural changes associated with dexamethasone-induced ocular hypertension in mice. *Invest. Ophthalmol. Vis. Sci.* **55**, 4922–4933 (2014).
31. D. E. Ingber, Mechanical signaling and the cellular response to extracellular matrix in angiogenesis and cardiovascular physiology. *Circ. Res.* **91**, 877–887 (2002).
32. F. J. Byfield, R. K. Reen, T. P. Shentu, I. Levitan, K. J. Gooch, Endothelial actin and cell stiffness is modulated by substrate stiffness in 2D and 3D. *J. Biomech.* **42**, 1114–1119 (2009).
33. W. D. Stamer, A. M. Williams, S. Pflugfelder, S. E. Coupland, Accessibility to and quality of human eye tissue for research: A cross-sectional survey of ARVO members. *Invest. Ophthalmol. Vis. Sci.* **59**, 4783–4792 (2018).
34. P. J. Anderson, J. Wang, D. L. Epstein, Metabolism of calf trabecular (reticular) meshwork. *Invest. Ophthalmol. Vis. Sci.* **19**, 13–20 (1980).
35. T. Borrás, L. L. Rowlette, E. R. Tamm, J. Gottanka, D. L. Epstein, Effects of elevated intraocular pressure on outflow facility and TIGR/MYOC expression in perfused human anterior segments. *Invest. Ophthalmol. Vis. Sci.* **43**, 33–40 (2002).
36. M. P. Fautsch, C. K. Bahler, D. J. Jewison, D. H. Johnson, Recombinant TIGR/MYOC increases outflow resistance in the human anterior segment. *Invest. Ophthalmol. Vis. Sci.* **41**, 4163–4168 (2000).
37. J. Gottanka, D. Chan, M. Eichhorn, E. Lütjen-Drecoll, C. R. Ethier, Effects of TGF-beta2 in perfused human eyes. *Invest. Ophthalmol. Vis. Sci.* **45**, 153–158 (2004).
38. J. A. Vranka, J. M. Bradley, Y. F. Yang, K. E. Keller, T. S. Acott, Mapping molecular differences and extracellular matrix gene expression in segmental outflow pathways of the human ocular trabecular meshwork. *PLoS One* **10**, e0122483 (2015).
39. M. D. Whale, A. J. Grodzinsky, M. Johnson, The effect of aging and pressure on the specific hydraulic conductivity of the aortic wall. *Biorheology* **33**, 17–44 (1996).

40. A. J. Sit, F. M. Coloma, C. R. Ethier, M. Johnson, Factors affecting the pores of the inner wall endothelium of Schlemm's canal. *Invest. Ophthalmol. Vis. Sci.* **38**, 1517–1525 (1997).
41. W. Ye, H. Gong, A. Sit, M. Johnson, T. F. Freddo, Interendothelial junctions in normal human Schlemm's canal respond to changes in pressure. *Invest. Ophthalmol. Vis. Sci.* **38**, 2460–2468 (1997).
42. P. A. Scott, Z. Lu, Y. Liu, H. Gong, Relationships between increased aqueous outflow facility during washout with the changes in hydrodynamic pattern and morphology in bovine aqueous outflow pathways. *Exp. Eye Res.* **89**, 942–949 (2009).
43. E. D. Cha, J. Xu, L. Gong, H. Gong, Variations in active outflow along the trabecular outflow pathway. *Exp. Eye Res.* **146**, 354–360 (2016).
44. M. Karnovsky, "A formaldehyde-glutaraldehyde fixative of high osmolality for use in electron microscopy" in *Fifth Annual Meeting of the American Society for Cell Biology*. https://www.researchgate.net/publication/244955881_A_Formaldehyde-Glutaraldehyde_Fixative_of_High_Osmolality_for_Use_in_Electron_Microscopy. Accessed 2 December 2019.
45. R. L. Moses, W. C. Claycomb, Ultrastructure of terminally differentiated adult rat cardiac muscle cells in culture. *Am. J. Anat.* **164**, 113–131 (1982).
46. M. Kroeber *et al*., Reduced expression of Pax6 in lens and cornea of mutant mice leads to failure of chamber angle development and juvenile glaucoma. *Hum. Mol. Genet.* **19**, 3332–3342 (2010).
47. H. A. Quigley, E. M. Addicks, W. R. Green, Optic nerve damage in human glaucoma. III. Quantitative correlation of nerve fiber loss and visual field defect in glaucoma, ischemic neuropathy, papilledema, and toxic neuropathy. *Arch. Ophthalmol.* **100**, 135–146 (1982).
48. A. T. Read, D. W. Chan, C. R. Ethier, Actin structure in the outflow tract of normal and glaucomatous eyes. *Exp. Eye Res.* **82**, 974–985 (2006).
49. J. W. Harding, I. N. Sneddon, The elastic stresses produced by the indentation of a plane surface of a semi-infinite elastic solid by a rigid punch. *Math. Proc. Camb. Philos. Soc.* **41**, 16–26 (1945).
50. A. R. Harris, G. T. Charras, Experimental validation of atomic force microscopy-based cell elasticity measurements. *Nanotechnology* **22**, 345102 (2011).
51. L. Sirghi, J. Ponti, F. Broggi, F. Rossi, Probing elasticity and adhesion of live cells by atomic force microscopy indentation. *Eur. Biophys. J.* **37**, 935–945 (2008).
52. K. D. Costa, Single-cell elastography: Probing for disease with the atomic force microscope. *Dis. Markers* **19**, 139–154 (2003–2004).
53. C. Y. Park *et al*., Mapping the cytoskeletal prestress. *Am. J. Physiol. Cell Physiol.* **298**, C1245–C1252 (2010).
54. B. D. Hoffman, G. Massiera, K. M. Van Citters, J. C. Crocker, The consensus mechanics of cultured mammalian cells. *Proc. Natl. Acad. Sci. U.S.A.* **103**, 10259–10264 (2006).
55. P. Cai *et al*., Quantifying cell-to-cell variation in power-law rheology. *Biophys. J.* **105**, 1093–1102 (2013).